OXFORD

Human Molecular Genetics, 2016, Vol. 25, No. 10 1885–1899

doi: 10.1093/hmg/ddw062
Advance Access Publication Date: 29 February 2016
Original Article

ORIGINAL ARTICLE

Pharmacokinetics, pharmacodynamics, and efficacy of a small-molecule *SMN2* splicing modifier in mouse models of spinal muscular atrophy

Xin Zhao[1,†], Zhihua Feng[2,†], Karen K. Y. Ling[2,†], Anna Mollin[1], Josephine Sheedy[1], Shirley Yeh[1], Janet Petruska[1], Jana Narasimhan[1], Amal Dakka[1], Ellen M. Welch[1], Gary Karp[1], Karen S. Chen[5], Friedrich Metzger[3], Hasane Ratni[3], Francesco Lotti[4], Sarah Tisdale[4], Nikolai A. Naryshkin[1], Livio Pellizzoni[4], Sergey Paushkin[5], Chien-Ping Ko[2,*] and Marla Weetall[1,*]

[1]PTC Therapeutics, Inc., South Plainfield, NJ 07080, USA, [2]Department of Biological Sciences, Section of Neurobiology, University of Southern California, Los Angeles, CA 90089, USA, [3]F. Hoffmann-La Roche, Pharmaceutical Research and Early Development, Roche Innovation Center Basel, Grenzacherstrasse 124, Basel 4070, Switzerland, [4]Department of Pathology and Cell Biology, Center for Motor Neuron Biology and Disease, Columbia University, New York, NY 10032, USA and [5]SMA Foundation, 888 Seventh Avenue, Suite 400, New York, NY 10019, USA

*To whom correspondence should be addressed. Tel: +1 9089129111 (M.W.)/+1 2137409182 (C.P.K.); Fax: +1 9082227231 (M.W.)/+1 2137405687 (C.P.K.); Email: mweetall@ptcbio.com (M.W.)/cko@usc.edu (C.P.K.)

Abstract

Spinal muscular atrophy (SMA) is caused by the loss or mutation of both copies of the survival motor neuron 1 (*SMN1*) gene. The related *SMN2* gene is retained, but due to alternative splicing of exon 7, produces insufficient levels of the SMN protein. Here, we systematically characterize the pharmacokinetic and pharmacodynamics properties of the SMN splicing modifier SMN-C1. SMN-C1 is a low-molecular weight compound that promotes the inclusion of exon 7 and increases production of SMN protein in human cells and in two transgenic mouse models of SMA. Furthermore, increases in SMN protein levels in peripheral blood mononuclear cells and skin correlate with those in the central nervous system (CNS), indicating that a change of these levels in blood or skin can be used as a non-invasive surrogate to monitor increases of SMN protein levels in the CNS. Consistent with restored SMN function, SMN-C1 treatment increases the levels of spliceosomal and U7 small-nuclear RNAs and corrects RNA processing defects induced by SMN deficiency in the spinal cord of SMNΔ7 SMA mice. A 100% or greater increase in SMN protein in the CNS of SMNΔ7 SMA mice robustly improves the phenotype. Importantly, a ∼50% increase in SMN leads to long-term survival, but the SMA phenotype is only partially corrected, indicating that certain SMA disease manifestations may respond to

[†]The authors wish it to be known that, in their opinion, the first three authors should be regarded as joint First Authors.
Received: October 27, 2015. **Revised:** January 25, 2016. **Accepted:** February 22, 2016

treatment at lower doses. Overall, we provide important insights for the translation of pre-clinical data to the clinic and further therapeutic development of this series of molecules for SMA treatment.

Introduction

Spinal muscular atrophy (SMA) is an autosomal recessive motor neuron disease with a spectrum of severity (1,2). Type I is the most severe and frequent form of SMA with disease onset occurring before 6 months of age and death usually by the age of two. Type II is the intermediate form of the disease with onset prior to 18 months of age. Type II patients never gain the ability to walk. Type III is the mild form characterized by onset after 18 months of age. Type III patients typically retain the ability to walk until later in life and have a normal life expectancy. SMA is caused by the mutation or deletion of both copies of the telomeric survival motor neuron 1 (*SMN1*) gene (3). About 95% of humans carry one or more copies of the paralogous *SMN2* gene (4). The protein-coding regions of *SMN1* and *SMN2* differ only in a translationally synonymous C-to-T transition at nucleotide 840, leading to alternative splicing and preferential exclusion of exon 7 from most of the mature *SMN2* transcripts (5,6). The resulting mRNA encodes an unstable SMNΔ7 protein that is rapidly degraded (7,8), while the low levels of full-length (FL) *SMN2* transcripts that include exon 7 produce small amounts of fully functional SMN protein. The severity of SMA is inversely correlated with *SMN2* gene copy number and SMN protein levels (9,10).

SMA is characterized by the loss of proximal spinal alpha motor neurons resulting in neuromuscular junction (NMJ) denervation, muscle atrophy and eventually death due to respiratory failure in severe Type I SMA patients (1,2,11). Proximal muscles are preferentially affected in the disease, as are the lower muscles more so than the muscles of the upper extremities. The differential vulnerability of distinct motor neuron pools in SMA is also demonstrated by the marked involvement of intercostal and axial muscles and the relative sparing of the diaphragm, which results in the characteristic bell-shaped chest and paradoxical breathing.

The SMN protein is part of a macromolecular complex that contains eight additional core proteins, termed Gemins 2–8 and Unrip [see (12) for a review]. The SMN complex is essential for the biogenesis of Sm-class small-nuclear ribonucleoproteins (snRNPs) of the major (U1, U2, U4 and U5) and minor (U11, U12 and U4atac) spliceosomes that carry out pre-mRNA splicing as well as for the assembly of U7 snRNP that functions in the 3′-end processing of intronless histone mRNAs (13). In addition to these well-established functions in snRNP assembly, SMN likely has other roles in RNA regulation the precise nature of which, however, remains poorly characterized (13). Additionally, while increasing evidence links dysregulation of RNA processing to SMA pathology, the mechanisms by which a deficit in the ubiquitously expressed SMN protein cause the loss of spinal cord motor neurons and other disease manifestations are not completely understood (1,2).

Since SMA is caused by reduced SMN protein levels, therapies that promote the inclusion of exon 7 in the *SMN2* mRNA are among the most promising approaches to treatment of SMA. The availability of mouse models has been instrumental in the pre-clinical development of experimental therapies for the disease (1,14,15). Accordingly, both antisense oligonucleotides (16–19) and small molecules (20–23) that promote inclusion of exon 7 into *SMN2* mRNA have been reported to correct the phenotype in mouse models of severe (Type I) SMA. We recently described three low-molecular weight compounds that selectively promote the inclusion of exon 7 in the *SMN2* mRNA to generate FL *SMN2* mRNA and increase SMN protein (20,23). These compounds increase life span, body weight gain and prevent disease-related motor dysfunction as well as neuromuscular deficits in the SMNΔ7 mouse model of SMA. Small-molecule SMN splicing modifiers have two key advantages over antisense oligonucleotide-based approaches: they can be dosed orally, as opposed to an injection into the spinal cord, and they distribute systemically and increase FL SMN protein expression in all tissues affected by SMA.

Here, we have better characterized one of these compounds (SMN-C1) to understand some of the parameters used in designing clinical trials, including the pharmacokinetic and pharmacodynamics relationships with SMN protein level increases, restoration of SMN-dependent gene expression deficits, and differences in the dose–response for various endpoints. We have also investigated potential biomarkers for efficacy. Our detailed characterization of SMN-C1 provides key information for the translation of pre-clinical data to the clinic.

Results

Pharmacokinetics of SMN-C1 in neonatal and adult mice

We performed a detailed pharmacokinetic evaluation of SMN-C1 in wild-type mice (Fig. 1). SMN-C1 was administered at a dose of 10 mg/kg to neonatal wild-type mice by intraperitoneal injection (IP) or to adult mice by oral gavage (PO). Neonatal mice [postnatal day 10 (PND10)] were dosed IP due to the difficulty in accurately dosing neonatal mice by oral gavage. As shown in Figure 1B, SMN-C1 plasma concentrations were similar in adult and neonatal mice through ~8 h, but the compound was eliminated more slowly from the neonatal mice than from the adult mice. Furthermore, concentrations of SMN-C1 in the brain were much higher in the neonatal mice than in the adult mice (Fig. 1C). For that reason, in subsequent survival studies, a lower dose was used in neonatal mice while the dose was increased for adult mice.

SMN-C1 increases SMN protein levels in mouse models of SMA

To define the pharmacokinetic parameters associated with pharmacodynamic responses as assessed by the increase in SMN protein levels (PK-PD), studies were performed in the C/C-allele mouse using various dosing regimens. This mouse has two SMN genes as a single allele (called the C allele): two copies of a hybrid gene in which murine *Smn1* gene is fused to human *SMN2* gene with a junction point in intron 6 and two copies of the full human *SMN2* gene located immediately downstream of the hybrid gene. The mice have a near-normal life span, but show decreased muscle function, reduced body weight gain, and peripheral necrosis in comparison with normal mice (24). The same total daily dose was administered via oral gavage either as a single dose or in two half doses 6 h apart. The maximal (peak) plasma concentration (C_{max}) was approximately twice as high when the total daily dose was given as a single bolus than when given as two half doses (data not shown). However, the

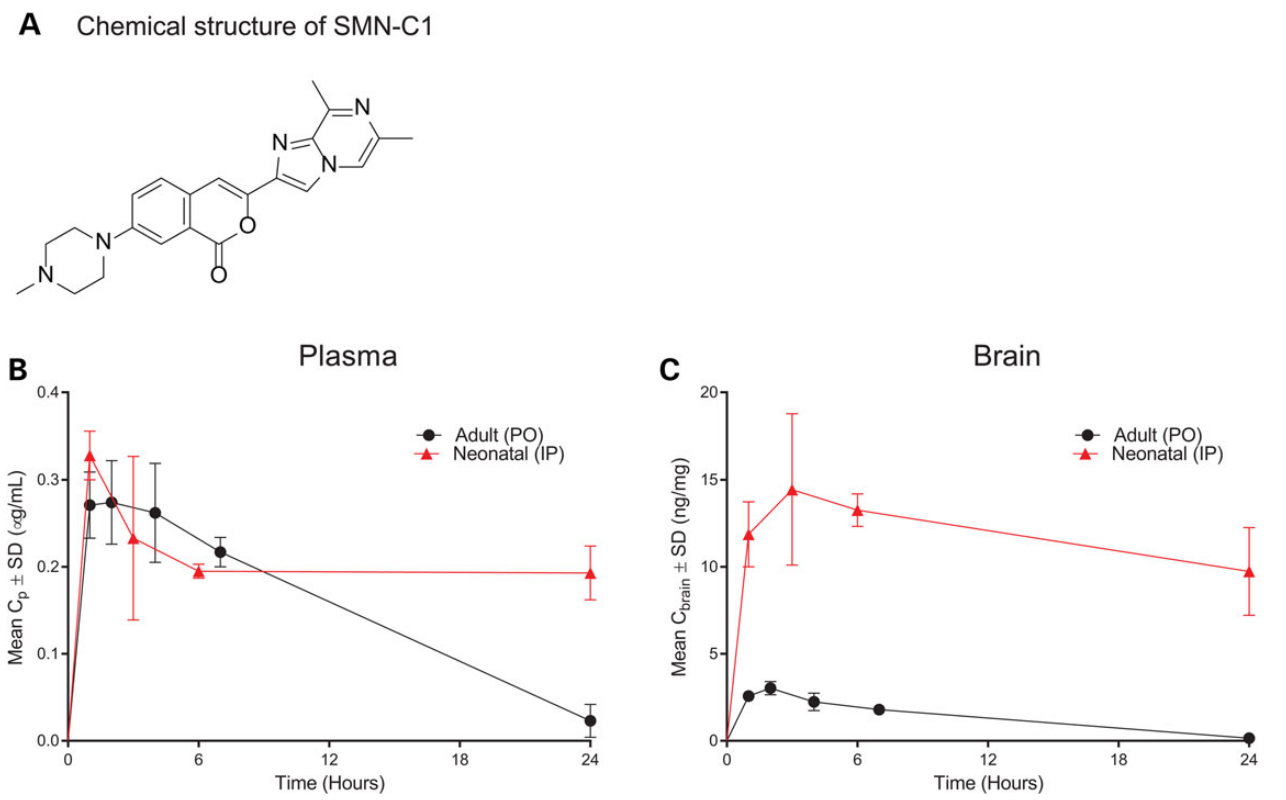

Figure 1. The chemical structure and pharmacokinetic profile of SMN-C1 in neonatal and adult mice. (**A**) The chemical structure of SMN-C1. (**B** and **C**) Twenty-four hour pharmacokinetic profile of SMN-C1 in plasma (B) and brain tissue (C) of wild-type neonatal and adult mice. SMN-C1 was administered IP at 10 mg/kg to neonatal (PND10) and by oral gavage (PO) at 10 mg/kg to adult (6 weeks old) FVB mice. Values at each time point represents the average of data from three mice ± SD.

total exposure as defined by the area under the plasma compound concentration versus time curve [area under the curve (AUC)] was similar for both dosing regimens (data not shown). Oral administration of SMN-C1 to C/C-allele SMA mice dose-dependently increased the levels of SMN protein in the spinal cord (Fig. 2A) and in peripheral blood mononuclear cells (PBMCs) purified from the blood of treated mice (Fig. 2B) compared with the levels of SMN protein in vehicle-dosed C/C-allele SMA mice. The increases in SMN protein were similar when the same total daily dose was administered either as a single bolus dose or in two half doses administered 6 h apart, suggesting that the pharmacodynamic response is associated with either the AUC or with the time above a threshold plasma concentration and not with the maximal plasma concentration (C_{max}). If C_{max} were the critical PK parameter, it is expected that the single bolus regimen would have been more effective than the split dose regimen of SMN-C1.

To determine whether the SMN-C1 distribution into both the periphery and the central nervous system (CNS) results in systemically increased FL SMN expression, we quantified SMN protein in the brain, spinal cord, quadriceps, skin, liver, heart as well as in PBMCs of SMN-C1-treated C/C-allele mice. We found that SMN protein levels increased in a dose-dependent manner in all tissues evaluated (Fig. 2A and B and Supplementary Material, Table S1) when compared with those in vehicle-dosed C/C-allele mice. The highest doses tested increased the levels of SMN protein above those measured in heterozygous (HET) control mice. Importantly, SMN protein levels in the spinal cord correlated well with those in the PBMCs (Fig. 2C), indicating that non-invasive measures of SMN protein in PBMC can be used to estimate SMN protein increases in the CNS.

We also evaluated SMN protein levels in neonatal SMNΔ7 SMA mice treated with SMN-C1. These mice lack the endogenous murine *Smn1* gene and have two copies of the human *SMN2* gene as well as six copies of the SMNΔ7 cDNA transgene. The mice die ~2 weeks after birth and are a model of severe SMA (25). In comparison with vehicle-dosed SMNΔ7 SMA mice, SMN protein levels in the brain, spinal cord, quadriceps, heart, liver and skin were elevated in a dose-dependent manner in SMNΔ7 SMA mice treated with SMN-C1 by IP injection once daily (qd) from PND3 through PND9 (Fig. 2D and E and Supplementary Material, Table S2). The levels of SMN protein measured in the spinal cord correlated well with the SMN protein levels measured in the skin (Fig. 2F), indicating that SMN protein increases in the skin, similar to increases in PBMCs, can also be used to estimate drug-mediated enhanced SMN expression in the CNS.

SMN-C1 corrects SMN-dependent snRNP biogenesis and RNA processing defects in SMA mice

Having demonstrated that SMN-C1 increases SMN protein, we investigated the effect of SMN-C1 treatment on the restoration of SMN protein function in SMA mice. The best-characterized activity of SMN is in the assembly of spliceosomal snRNPs (13), the core constituents of the spliceosome that carry out pre-mRNA splicing. Furthermore, it is well-established that spliceosomal snRNP biogenesis is disrupted in SMA mice leading to alterations in the steady-state levels of spliceosomal snRNAs (26,27). Therefore, we determined if SMN-C1 treatment restores spliceosomal snRNA levels in SMA mice. SMNΔ7 SMA mice were treated with SMN-C1 at a dose of 3 mg/kg by IP administration from PND3 through PND11 followed by the collection of the spinal cord at

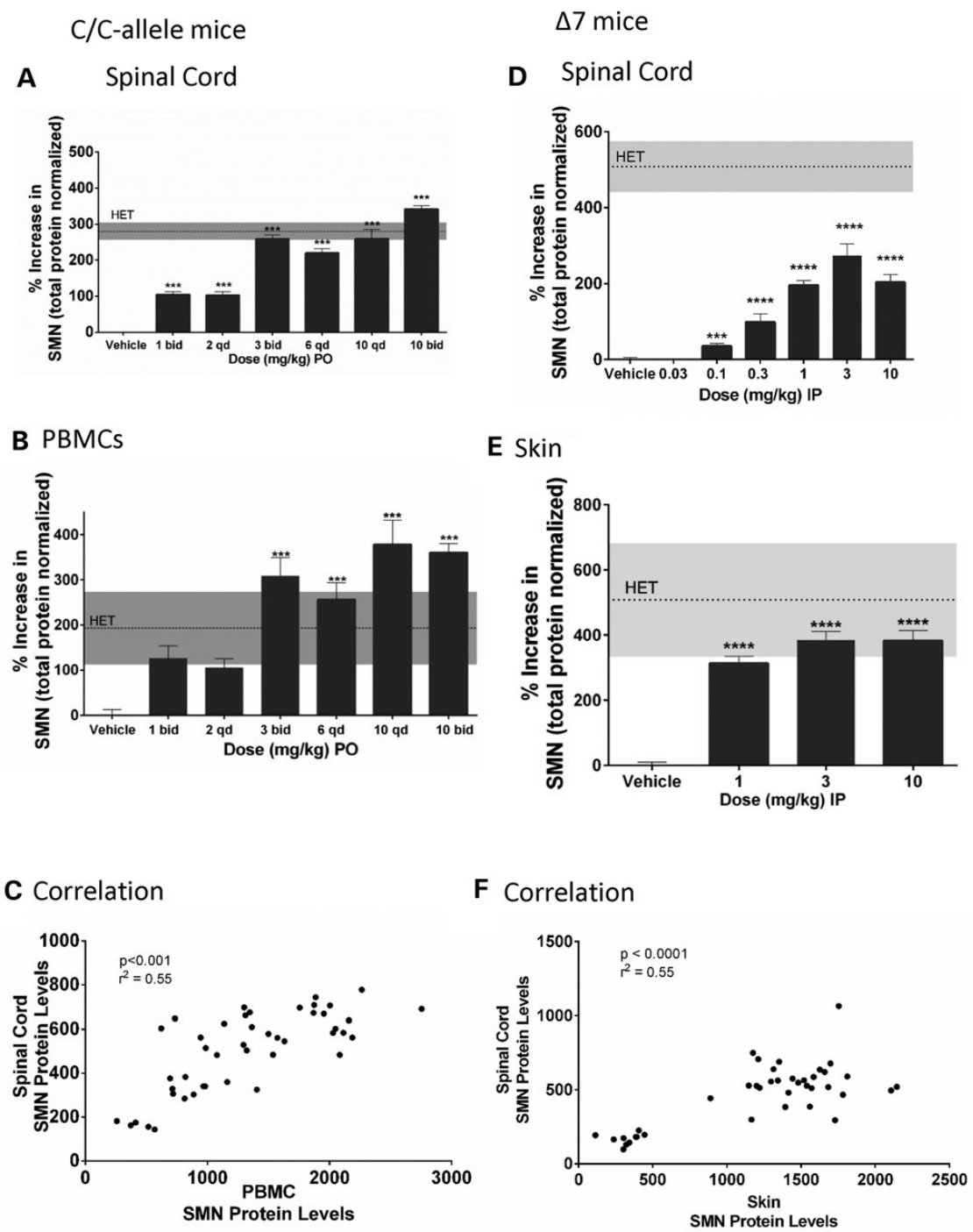

Figure 2. SMN-C1 increases SMN protein in the CNS and in peripheral tissue in two mouse models of SMA. Percent increase in SMN protein levels relative to vehicle-dosed in the C/C-allele (**A–C**) or in SMNΔ7 SMA (**D–F**) mouse models of SMA. C/C-allele mice were dosed for 10 days by oral gavage with SMN-C1 daily either once per day (qd) or twice per day (bid) and euthanized 1 h after the last dose. SMNΔ7 SMA mice were dosed once daily from PND3 through PND9 and euthanized 1 h after the last dose on PND9. Data are shown as the percent increase above the mean SMN levels measured in vehicle-dosed mice. (A and B) Values represent the mean of five mice per group (±SEM). (D and E) The number of mice per group are as follows: vehicle ($N = 22$), 0.03 mg/kg ($N = 6$), 0.1 mg/kg ($N = 6$), 0.3 mg/kg ($N = 5$), 1 mg/kg ($N = 13$), 3 mg/kg ($N = 9$) and 10 mg/kg ($N = 8$). The dashed lines in (A, B, D, and E) represent the mean levels of SMN protein increase (±SEM, shaded areas) measured in HET littermates. (A and D) The SMN protein level increases in the spinal cord. (B) The SMN protein level increases in purified PBMCs. (C) Correlation between PBMC SMN protein levels and spinal cord SMN protein levels. Each point represents an individual mouse. (E) SMN protein levels in the skin. (F) Correlation between skin SMN protein levels and spinal cord SMN protein levels. Each point represents an individual mouse. ***$P < 0.001$ and ****$P < 0.0001$ (ANOVA, multiple comparisons versus vehicle).

PND11 for RNA analysis. First, we confirmed that splicing of the human *SMN2* transgene was robustly corrected leading to increased FL *SMN2* mRNA levels (Fig. 3A) and that expression of SMN protein in the spinal cord was increased (Fig. 3B) in comparison with those in the vehicle-dosed SMNΔ7 SMA mice. Consistent with previous studies demonstrating a preferential disruption in

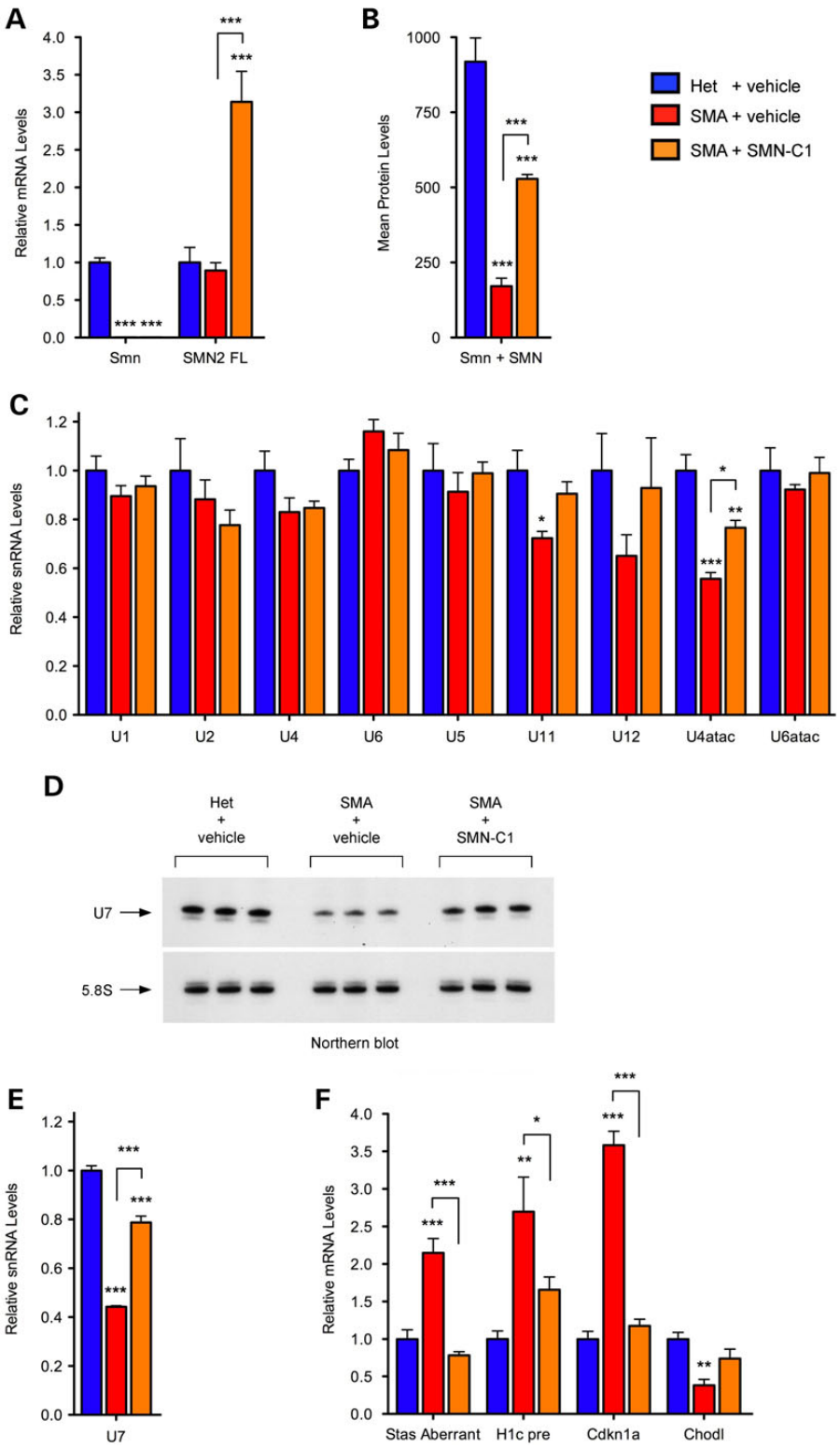

Figure 3. SMN-C1 corrects SMN-dependent snRNP biogenesis and RNA processing defects in SMA mice. Control HET mice (blue) were dosed with vehicle and SMNΔ7 SMA mice were dosed with either vehicle (red) or 3 mg/kg SMN-C1 (orange) from PND3 through PND11 and euthanized 1 h after dosing on PND11. Data represent means ± SD. Spinal cord tissues were analyzed as follows: (**A**) RT-qPCR analysis of mouse *Smn1* and FL human *SMN2* mRNAs. (**B**) Levels of SMN protein. (**C**) RT-qPCR analysis of spliceosomal snRNAs. (**D**) Northern blot analysis of U7 snRNA. (**E**) Quantification of U7 snRNA levels from the northern blot analysis in (D). Data were normalized to 5.8S rRNA and expressed relative to HET controls. (**F**) RT-qPCR analysis of mRNAs that are dependent on functional SMN protein for proper processing (see text for further details). Unless otherwise indicated, statistics were performed to determine the significance of the difference between HET (shown in blue) and the other treatment groups. $^{*}P < 0.05$, $^{**}P < 0.01$ and $^{***}P < 0.001$ (ANOVA, multiple pair-wise comparisons).

the minor snRNP levels in tissues of SMA mice (26,27), reverse transcriptase–quantitative polymerase chain reaction (RT-qPCR) analysis revealed a reduction in the levels of U11, U12 and U4atac minor spliceosomal snRNAs—but not in the levels of the major snRNAs—in the spinal cord of SMNΔ7 SMA mice (Fig. 3C). Importantly, treatment with SMN-C1 increased the levels of U11, U12 and U4atac snRNAs in the spinal cord of SMA mice (Fig. 3C). In addition to spliceosomal snRNPs, the SMN complex is also required for the assembly of U7 snRNP (13), an RNP that functions not in splicing, but in the 3′-end processing of histone mRNAs. Since SMN-mediated U7 snRNP assembly is disrupted by SMN deficiency *in vivo* (28), we investigated the effect of SMN-C1 on U7 snRNP biogenesis in SMA mice. Northern blot analysis confirmed the strong reduction in U7 snRNA levels in the spinal cord of SMA mice and, more importantly, revealed robust U7 restoration upon treatment with SMN-C1 (Fig. 3D and E). Together, these results demonstrate that SMN-C1 treatment markedly increases SMN functions in the biogenesis of both spliceosomal snRNPs and U7 snRNP in SMA mice.

Beyond decreased snRNA expression, several mRNA processing changes have been documented in SMA mice that have been attributed to defects in distinct SMN-dependent pathways (13). Accumulation of aberrantly spliced mRNA of the U12 intron-containing gene *Stasimon* (*Stas*) in SMA mice provides a measure of minor snRNP dysfunction (29). Increased levels of 3′-extended *histone H1c* mRNA reflect disruption of U7 snRNP-dependent 3′-end processing of histone mRNAs induced by SMN deficiency (28). Up-regulation of the cyclin-dependent kinase inhibitor 1A mRNA—which is particularly prominent within SMA motor neurons (30)—and reduced expression of the motor neuron-specific *Chondrolectin* (*Chodl*) mRNA are additional RNA changes that occur in SMA mice possibly due to altered mRNA stability rather than snRNP dysfunction (13,31). Furthermore, altered *Stas* and *Chodl* expression have been shown to contribute to motor neuron dysfunction in Drosophila and zebrafish models of SMA (29,32). Importantly, RT-qPCR analysis demonstrated that all of these SMN-dependent RNA changes are robustly corrected in the spinal cord of SMA mice by SMN-C1 treatment (Fig. 3F). Collectively these findings demonstrate that *in vivo* SMN-C1 increases levels of functional SMN and restores downstream RNA processing events regulated by SMN.

SMN-C1 improves survival, body weight, phenotype and motor behavior in SMA mice

Having demonstrated the ability of SMN-C1 to increase SMN protein expression and function in the SMNΔ7 mouse model of SMA, we defined the relationship between dose and amelioration of SMA-like disease phenotypes in two separate studies. In the first study, SMN-C1 was administered daily at doses of 0.1 mg/kg IP from PND3 through PND23 and 0.6 mg/kg PO starting on PND24. The median survival time for mice dosed with vehicle was 18 days and all of these mice died by PND22 (Fig. 4A). In sharp contrast, SMN-C1 treatment increased survival at both the 0.1 mg/kg IP PND3–23 → 0.6 mg/kg/day PO and 0.3 mg/kg IP PND3–23 → 2 mg/kg/day PO dose regimens with 64% (7/11) and 67% (8/12) of the mice surviving, respectively, at PND120 when the study was terminated. As shown in Figure 4B, vehicle-dosed mice initially gained weight, but then stopped and lost weight before dying. The mean maximum weight of ∼5 g was reached on PND11. In contrast, mice dosed with SMN-C1 gained weight, although slightly less than did the HET mice. The higher dose (0.3 mg/kg IP → 2 mg/kg PO) tended to be more effective than was the lower dose tested (0.1 mg/kg IP → 0.6 mg/kg PO) at promoting body weight gain.

Administration of SMN-C1 improved the general appearance of the SMA mice as evidenced by comparing PND71 mice treated with SMN-C1 and age-matched HET mice (Supplementary Material, video). The video footage shows SMNΔ7 SMA mice at PND71 treated with SMN-C1 and age-matched HET mice, with SMA mice at the higher dose appearing essentially normal while those at the lower dose noticeably lacking tails. SMA mice develop necrosis of the tail, which is eventually lost (33). Furthermore, in SMNΔ7 SMA mice treated with gene therapy administered directly to the CNS, survival was extended, but due to the lack of SMN induction in peripheral tissues the tails of the mice were necrotic and extremely short (34,35). These studies indicate that the tail length can be used as a measure of peripheral SMN protein expression. We found that despite similar long-term survival, the tails of mice administered the lower dose (0.1 mg/kg IP → 0.6 mg/kg PO) were shorter than those of the mice dosed administered higher dose (0.3 mg/kg IP → 2 mg/kg PO) (Fig. 4C and D). When normalized for body weight, tails of the mice administered the higher dose of SMN-C1 (0.3 mg/kg IP → 2 mg/kg PO) were similar in length to those of the HET mice(Supplementary Material, Fig. S1A). However, even when normalized for reduced body weight, the tail length of the mice in the lower dose group (0.1 mg/kg IP → 0.6 mg/kg PO) was reduced when compared with that of the HET mice (Supplementary Material, Fig. S1A). Similarly, semi-quantitative evaluation demonstrated that necrosis of the tissues surrounding the eye and the pinna evident in mice given the lower dose (0.1 mg/kg IP → 0.6 mg/kg PO), but not in mice given the higher dose (0.3 mg/kg IP → 2 mg/kg PO) (Supplementary Material, Fig. S1B).

A second study was conducted to assess efficacy of higher doses. In this study, SMN-C1 was administered at doses of 1, 3 or 10 mg/kg IP from PND3 through PND23. From PND24 through the end of the study, SMN-C1 was administered at 6, 20 or 60 mg/kg/day PO. These doses were no more effective in promoting survival or body weight gain or in improving motor function than were the lower doses (Fig. 4E and F, Supplementary Material, Fig. S2).

SMN-C1 prevents motor neuron loss and rescues synaptic pathology in SMA mice

Next, we investigated the effects of SMN-C1 on the hallmark tissue pathologies of SMA (1,2). Tissues were evaluated at PND14 because a sufficient number of vehicle-dosed SMNΔ7 SMA mice were still alive at this age. As in humans, spinal motor neurons degenerate in SMNΔ7 SMA mice. As shown in Figure 5A, the number of motor neurons in the spinal cord was reduced in vehicle-dosed SMNΔ7 SMA mice compared with the number in the HET control [$P < 0.001$, one-way analysis of variance (ANOVA), multiple comparisons versus vehicle]. SMN-C1 injected IP from PND3 through PND14 increased the motor neuron number in a dose-dependent manner, resulting in a similar number of motor neurons in the spinal cords of SMNΔ7 SMA mice treated with 3 mg/kg SMN-C1 as in the HET mice ($P < 0.001$, ANOVA, multiple comparisons versus vehicle). In addition, lumbar motor neurons displayed a decrease in the number of proprioceptive primary afferents abutting onto the somata and proximal dendrites in the SMNΔ7 SMA mice compared with those in controls (36,37). VGluT1 is a marker of proprioceptive synapses motor neurons. In mice treated with SMN-C1, the number of vGluT1 inputs onto L3–5 motor neuron somata was increased relative to that in vehicle-treated SMA mice and similar to that of the HET

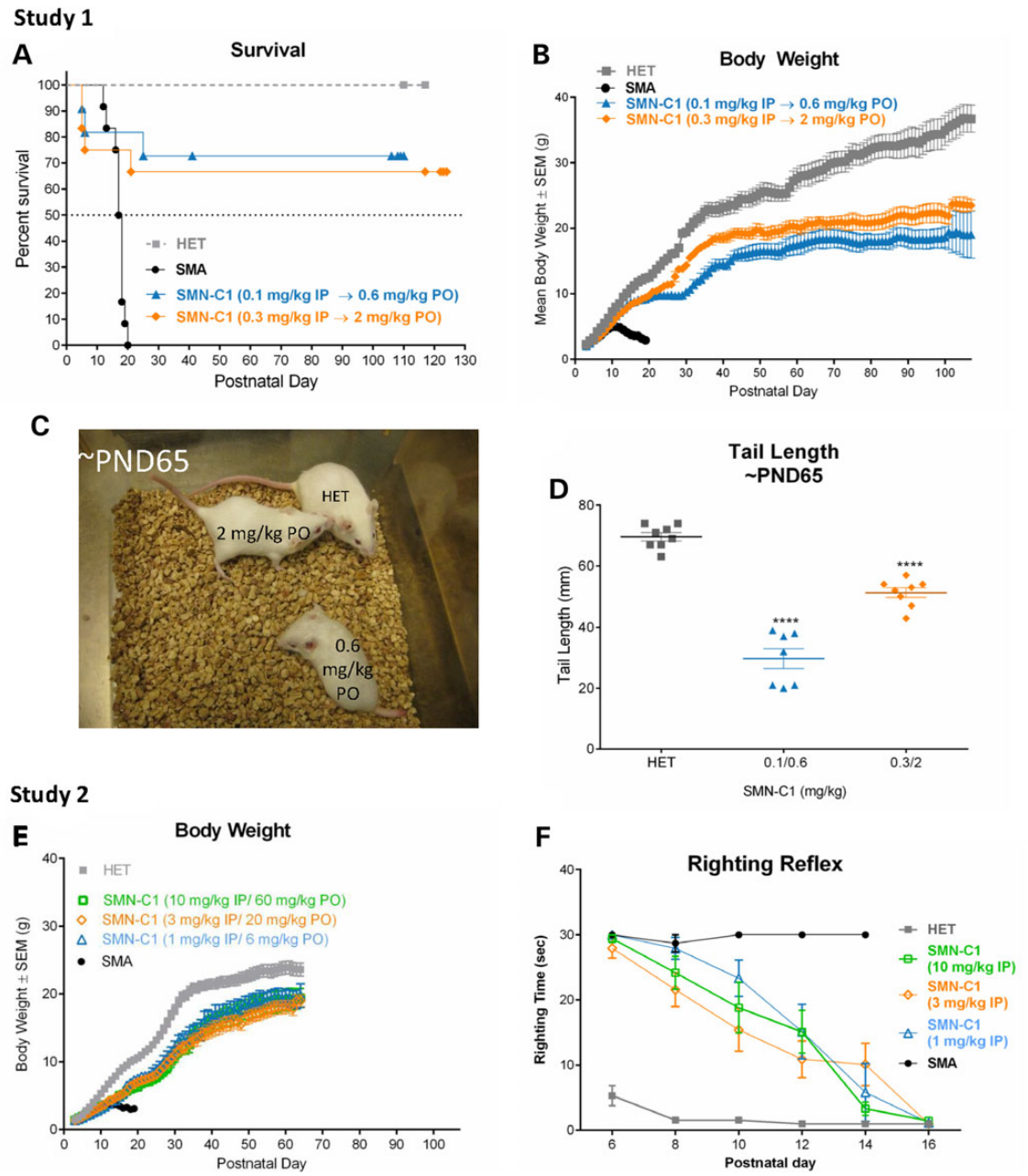

Figure 4. Administration of SMN-C1 increases survival and body weight gain, improves motor function, and reduces tissue necrosis in SMNΔ7 SMA mice. For Study 1 (**A–D**): animals were treated with vehicle or SMN-C1 at doses of 0.1 or 0.3 mg/kg/day from PND3 to PND23 by IP injection, and thereafter by oral gavage at doses of 0.6 or 2 mg/kg/day from PND24 through PND120. Data represent means ± SEM of an initial group size of 10 (HET) and 15 (SMNΔ7 SMA mice, labeled SMA or SMN-C1 treated) animals per data point. (A) Kaplan–Meier survival plot. (B) Body weight from PND3 to PND120. (C) Photograph of treated SMNΔ7 SMA mice on ~PND65. SMAΔ7 mice were treated with 0.1 mg/kg IP/0.6 mg/kg PO (labeled 0.6 mg/kg) or 0.3 mg/kg IP/ 2 mg/kg PO (labeled 2 mg/kg PO). An age-matched littermate HET for mouse *Smn1* (labeled HET) is shown for comparison purposes. (D) Tail length of mice measured on ~PND65. For Study 2 (**E** and **F**): animals were treated with vehicle or SMN-C1 from PND3 to PND23 by IP injection, and thereafter by oral gavage through PND64 at which time the study was stopped. Data represent means ± SEM with initial group size of 9 HET littermates, 11 vehicle-dosed SMNΔ7 SMA mice, 13 SMNΔ7 SMA mice treated with SMN-C1 at 1 mg/kg IP → 6 mg/kg/day PO, 14 SMAΔ7 mice treated with SMN-C1 at 3 mg/kg IP → 10 mg/kg/day PO and 12 SMNΔ7 SMA mice treated with SMN-C1 at 10 mg/kg IP → 60 mg/kg/day PO. (E) Body weight from PND3 to PND64. (F) Latency to righting (in seconds) in neonatal SMNΔ7 SMA mice. $^{**}P < 0.01$, $^{***}P < 0.001$ and $^{****}P < 0.0001$ (ANOVA, multiple comparisons versus HET).

mice (Fig. 5B; $P < 0.0001$, one-way ANOVA, multiple comparisons versus vehicle). Together these results demonstrate that SMN-C1 prevented the loss of motor neurons as well as the loss of proprioceptive synaptic inputs onto motor neurons somata.

In addition to the effect on motor neurons in the spinal cord, another major pathology of SMA is the loss of the NMJ in select vulnerable muscles (1,2,36–38). In SMNΔ7 SMA mice, denervation of NMJs is most evident in a group of clinically relevant muscles that are most vulnerable to the disease including the *longissimus capitis* and the *splenius capitis* muscle (38). In contrast, NMJs in resistant muscles such as the *extensor digitorum longus* (EDL) and *sternomastoid* muscles, remain almost fully innervated even at the disease end-stage (36,38). To assess the effect of SMN-C1 at the NMJ, we examined the morphology and physiology of NMJs

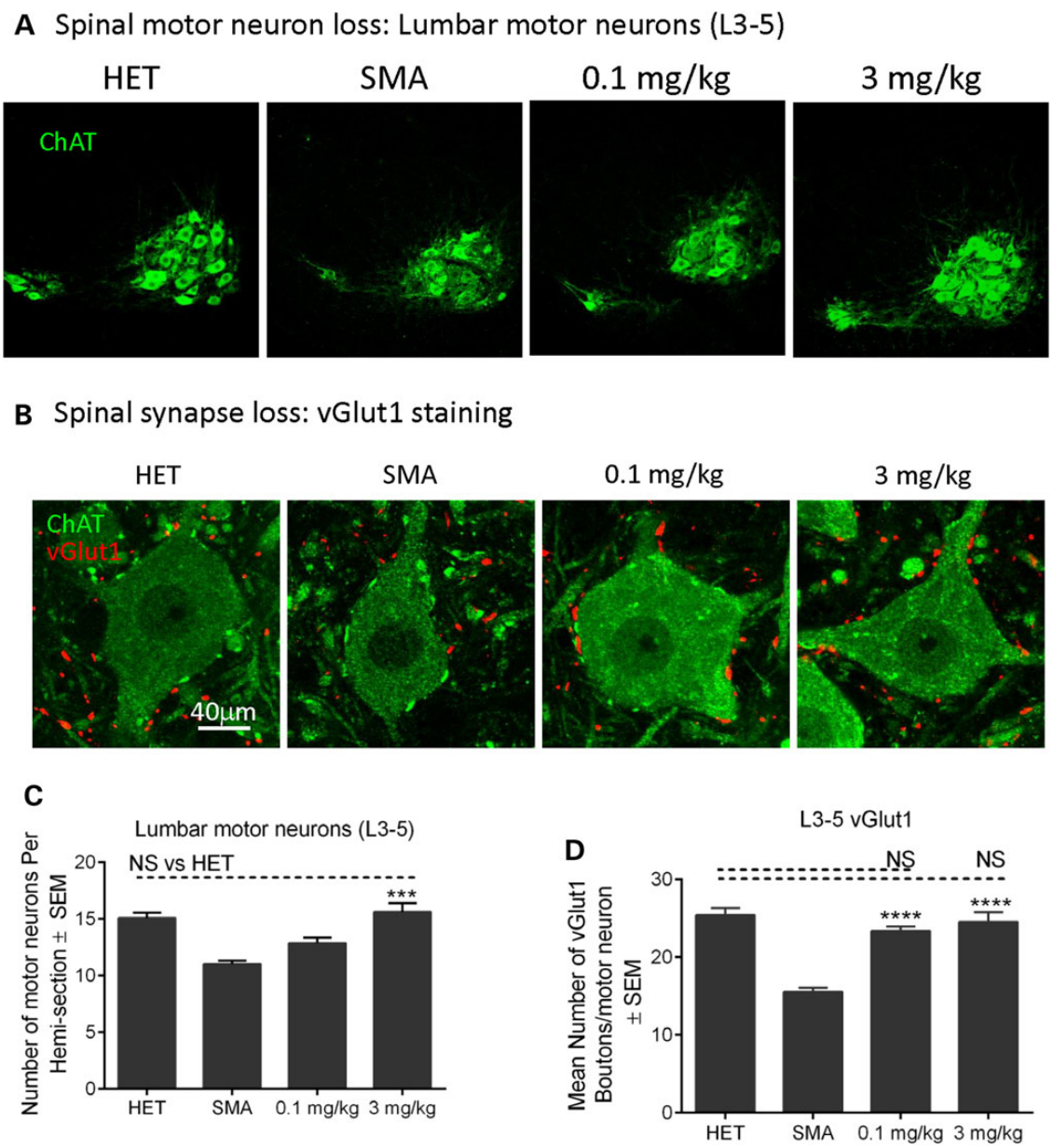

Figure 5. SMN-C1 prevents loss of motor neurons and proprioceptive synapses onto motor neurons in the spinal cord. Animals were treated by IP injection with vehicle or SMN-C1 at doses of 0.1 or 3 mg/kg/day from PND3 to PND14. (**A**) Representative images of lumbar motor neurons in the L3–5 sections of the spinal cord. (**B**) Representative image of vGlut1-positive somal synapses. (**C**) Quantification of lumbar motor neurons in the L3–5 section of the spinal cord (HET $N = 4$; SMNΔ7 SMA $N = 5$; 0.1 mg/kg $N = 5$, 3 mg/kg $N = 5$). (**D**) Quantification of the number of vGlut1-positive somal synapses (HET $N = 4$; SMNΔ7 SMA $N = 4$; 0.1 mg/kg $N = 5$, 3 mg/kg $N = 5$). ***$P < 0.001$ and ****$P < 0.0001$ (ANOVA, multiple comparisons versus SMA control). NS = not significant (ANOVA, multiple comparisons versus HET).

in the *longissimus capitis* muscle of SMNΔ7 SMA mice. As shown in Figure 6A and B, NMJs in the *longissimus capitis* of SMNΔ7 SMA mice were largely denervated (only ~20% fully innervated) at PND14. In contrast, in mice dosed with SMN-C1 at 3 mg/kg IP (from PND3 through PND14), over 65% of NMJs in the *longissimus capitis* were fully innervated (Fig. 6B). Similarly, only ~44% of NMJs are fully innervated in the *splenius capitis* muscle from vehicle-dosed SMNΔ7 SMA mice (Supplementary Material, Fig. S3, HET versus SMA), while fully innervated in SMNΔ7 SMA mice dosed with SMN-C1 at 3 mg/kg IP (from PND3 through PND14) (Supplementary Material, Fig. S3, SMN-C1 treated versus SMA).

In mouse models of SMA, the pre-synaptic nerve terminals contain an abnormal accumulation of neurofilaments (NF) at the NMJ (39–41). As shown in the SMA-resistant *sternomastoid* muscle (Fig. 6C), while no NF accumulation occurred in HET mice, 88% of the NMJs had NF accumulation in vehicle-treated SMNΔ7 SMA mice. This accumulation was reduced by 19 and 94%, respectively, following treatment with doses of 0.1 mg/kg and of 3 mg/kg SMN-C1.

To examine transmission at the NMJ in SMNΔ7 SMA mice, we first performed intracellular recording in the resistant EDL muscle. Muscle contraction was prevented by pre-incubation with µ-conotoxin, which blocks voltage-gated sodium channels in muscle (42). The NMJ of the SMNΔ7 SMA EDL muscle showed a significantly reduced spontaneous miniature endplate potential (MEPP) frequency and increased MEPP amplitude [Supplementary Material, Fig. S4; (36)]. The increase in MEPP amplitude may be due to the higher input resistance of the smaller SMNΔ7

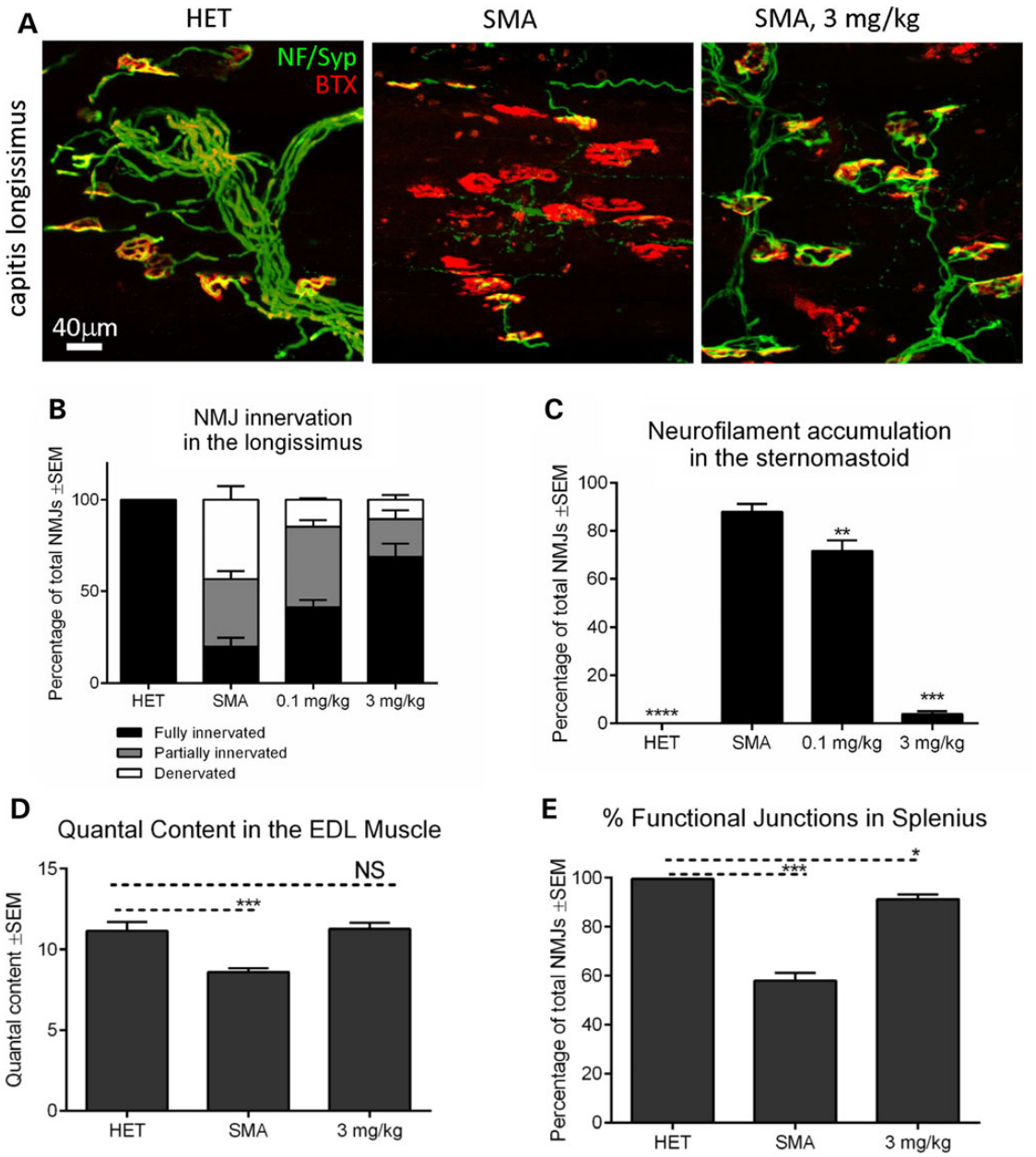

Figure 6. SMN-C1 treatment improves NMJ morphology and synaptic efficiency. Animals were treated by IP injection with vehicle or SMN-C1 at doses of 0.1 or 3 mg/kg/day from PND3 to PND14. (**A**) Representative images of the NMJ of the *longissimus capitis* muscle: HET mice, vehicle-dosed SMNΔ7 SMA mice and SMN-C1-treated SMNΔ7 SMA mice. Green (NF), green (synaptophysin), red (α-bungarotoxin) and yellow is formed where the synaptophysin (nerve terminals, green) and α-bungarotoxin(muscle, red) overlap. (**B**) Quantification of the percentage of fully and partially innervated NMJs in the *longissimus capitis* (HET $N = 6$; vehicle $N = 6$; 0.1 mg/kg $N = 4$, 3 mg/kg $N = 5$). (**C**) Quantification of NF accumulation in the *sternomastoid* muscle (HET $N = 5$; vehicle $N = 5$; 0.1 mg/kg $N = 4$, 3 mg/kg $n = 5$). (**D**) Quantification of quantal content in the EDL muscle of HET mice, SMNΔ7 SMA vehicle-dosed and SMN-C1-treated SMNΔ7 SMA mice. (**E**) Quantification of functional NMJs of HET mice, SMNΔ7 SMA vehicle-dosed and SMN-C1-treated SMNΔ7 SMA mice ($N = 5$ per group). *$P < 0.0001$ (ANOVA, SMNΔ7 SMA versus SMN-C1-treated SMNΔ7 SMA and SMNΔ7 SMA versus HET). Differences between SMN-C1-treated SMNΔ7 SMA and HET were not statistically significant.

SMA mouse muscle fibers (Fig. 7). The amplitude of evoked endplate potentials (EPPs) was similar between control and SMNΔ7 SMN NMJs (Supplementary Material, Fig. S4). Correspondingly, quantal content, calculated by dividing the amplitude of EPP by MEPP (43), was reduced by ~25% in SMNΔ7 SMA mouse NMJs compared with those in the HET mice (Fig. 6D, HET versus SMA). Therefore, despite the full NMJ innervation of the EDL muscle, synaptic transmission in EDL NMJs is defective as demonstrated by reduced quantal content. Treatment with SMN-C1 at a dose of 3 mg/kg corrected the amplitude and frequency of MEPPs, as well as the quantal content indicating that both the morphology and function of the NMJ were improved with SMN-C1 treatment.

In addition to the resistant EDL muscle, we also examined NMJ function in the vulnerable *splenius capitis* muscle. NMJs that exhibit an EPP upon nerve stimulation are defined as functional junctions. At PND14, all of the NMJs in HET mice were functional as demonstrated by the presence of EPPs upon nerve stimulation (Fig. 6E). In contrast, only 58% ($P < 0.0001$ for vehicle-dosed SMA mice versus HET) of the endplates in the *splenius capitis* of SMNΔ7 SMA mice displayed EPPs upon nerve stimulation,

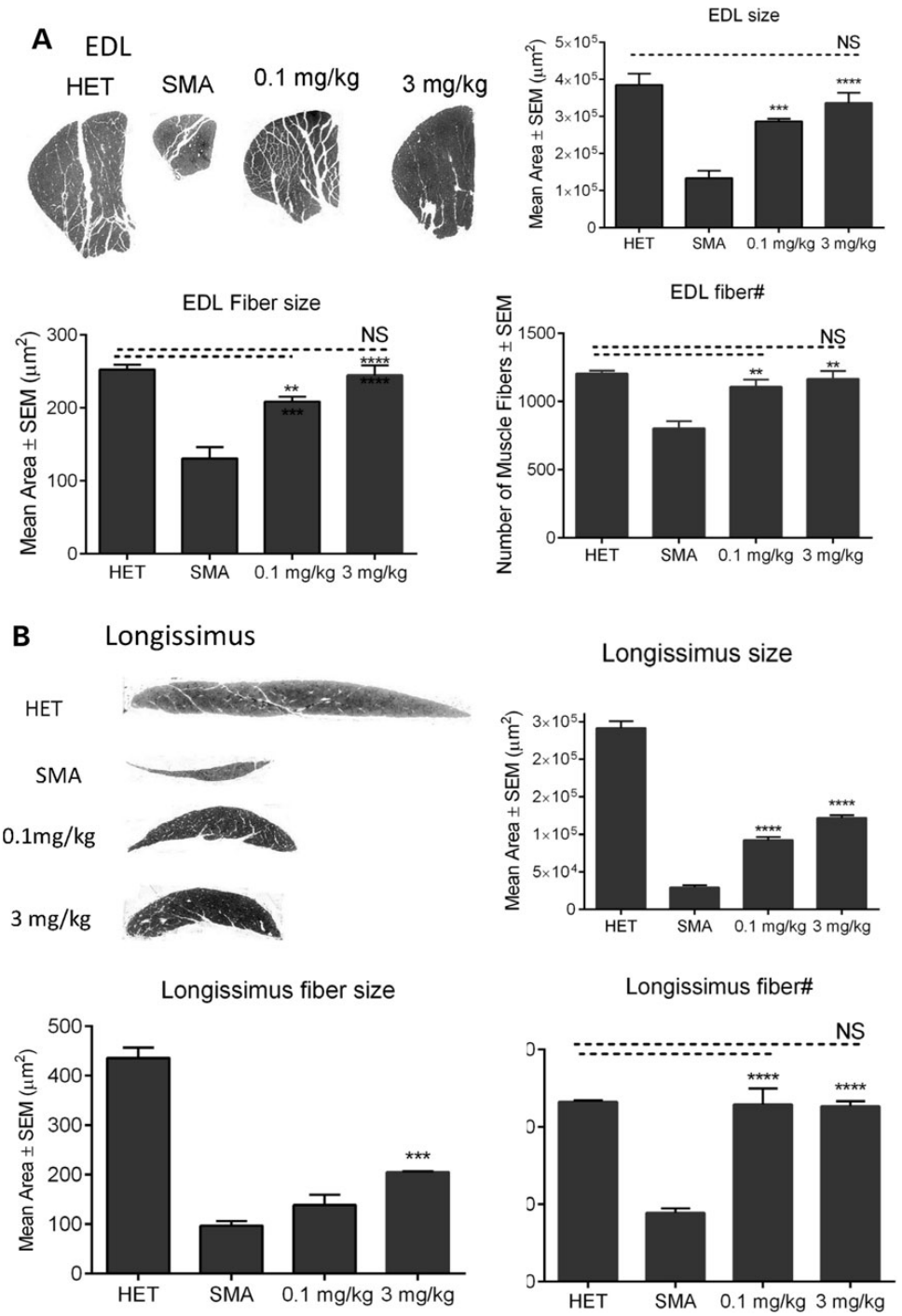

Figure 7. SMN-C1 reduces muscle atrophy. Animals were treated by IP injection with vehicle or SMN-C1 at doses of 0.1 or 3 mg/kg/day from PND3 to PND14. HET mice, vehicle-dosed SMNΔ7 SMA mice and SMN-C1-treated SMNΔ7 SMA mice. (**A**) EDL, (**B**) Longissimus: images of the muscle, quantification of the area of the muscle, quantification of the number of myofibers and quantification of myofiber size in the muscle.

indicating that ~42% of junctions are silent. This result is consistent with our morphological analysis of *splenius capitis* muscle NMJ innervation showing that 45% of junctions are denervated in this muscle (Supplementary Material, Fig. S3). SMN-C1 treatment increased the functional junctions to 91% ($P < 0.05$ for SMN-C1-treated versus vehicle-dosed SMA mice) and increased innervation (Supplementary Material, Fig. S3). Together, our findings demonstrate that SMN-C1 improves NMJ synaptic transmission efficacy in both resistant and vulnerable muscles.

SMN-C1 corrects muscle atrophy in SMA mice

A striking manifestation of SMA in both animal models and patients is muscle atrophy (1,2). As shown in Figure 7, the total cross-sectional area of the EDL muscle in SMNΔ7 SMA mice was reduced by 65% compared with that of the HET littermates at PND14. Treatment with SMN-C1 at doses of 0.1 or 3 mg/kg from PND3 through PND14 resulted in 115 and 152% increases, respectively, in the size of EDL muscles relative to those in the vehicle-dosed

SMNΔ7 SMA mice (Fig. 7A). When treated with a dose of 3 mg/kg SMN-C1, the EDL cross-sectional area was not significantly different from that of HET littermates. This overall increase in muscle size reflects an increase in the myofiber size and myofiber number (Fig. 7A). Additionally, treatment with SMN-C1 at doses of 0.1 or 3 mg/kg resulted in ∼2- and ∼3-fold increases, respectively, in the size of the vulnerable *longissimus capitis* muscle (Fig. 7B). This was associated with a correspondingly large increase in the size and number of muscle fibers. Thus, SMN-C1 treatment results in a dose-dependent amelioration of muscle atrophy in SMA mice.

Discussion

Here, we have characterized SMN-C1, a low-molecular weight compound that corrects alternative splicing defects of *SMN2* exon 7. We evaluated SMN-C1 pharmacokinetics in mice, the dose–response of SMN-C1 induction of SMN protein in two mouse models of SMA, the correlation between SMN-C1 PK and SMN protein induction *in vivo*, and demonstrated that the peripheral SMN protein levels correlated with CNS SMN protein levels in the C/C-allele and SMNΔ7 mouse models of SMA. Importantly, increased SMN protein expression and function are further indicated by robust correction of SMN-dependent RNA processing pathways that are dysregulated in SMA. Further, we showed that administration of SMN-C1 to SMNΔ7 SMA mice resulted in long-term survival of >60% of the mice, increased body weight, and an improved phenotype. These results can be used to guide design of clinical trials aimed to show efficacy of compounds that modify the alternative splicing of *SMN2* exon 7 for use in the treatment of SMA patients.

SMN-C1 showed excellent distribution into the CNS and peripheral tissues when administered systemically to both neonatal and adult mice. CNS and plasma exposures were higher in neonatal mice. The blood–brain barrier is not fully mature in the mouse at PND10 (44), which may account for the higher CNS exposure to SMN-C1 in neonatal mice in comparison with adult mice. The longer terminal half-life in plasma of neonatal mice may be due to decreased compound clearance, consistent with prior evidence that enzymes responsible for xenobiotic elimination such as cytochrome P450 enzymes are not expressed in neonatal mice (45,46). In neonatal mice, a daily dose was sufficient for sustained exposures. At PND24, the dose was increased and administered twice per day 6 h apart. Comparison of once-daily versus twice daily dosing of the same total quantity of the compound demonstrated that SMN protein induction correlates more with AUC or time above a threshold plasma concentration, and less with C_{max}. Consistent with the tissue distribution of SMN-C1 *in vivo*, administration of SMN-C1 in mouse models of SMA increased SMN protein in all tissues evaluated. Although SMA is characterized by the loss of motor neurons in the spinal cord, additional studies have highlighted systemic pathology including cardiovascular pathology, peripheral necrosis, pancreatic and liver deficiencies in mouse models of the disease (16,47–50) as well as in SMA patients (49–52). For example, the peripheral delivery of antisense oligonucleotides that promote *SMN2* exon 7 inclusion improves survival rates in mouse models of SMA, although not as much as central delivery. Importantly, the delivery of antisense oligonucleotides to both the CNS and the periphery was most effective (16). In a recent study, increasing SMN only in the peripheral tissues rescued peripheral necrosis in a mouse model of mild SMA and extended survival in a severe mouse model of SMA (17). Therefore, the SMN-C1-induced increases in SMN protein in both the periphery (quadriceps, heart, liver, skin and PBMCs: supplementary Material, Tables S1 and S2) and the CNS (brain, spinal cord: supplementary Material, Tables S1 and S2) indicate that the likelihood of clinical success is expected to be higher for compounds with both central and systemic activity such as SMN-C1 when compared with therapies that are restricted to either the CNS or to the periphery. Additionally, we show that increases in SMN protein levels in the PBMCs and the skin correlate with the increases of SMN protein levels in the brain and spinal cord. This indicates that peripheral tissues such as blood, skin or muscle, which can be collected in a relatively non-invasive way, could be analyzed to evaluate SMN increases in the CNS.

We demonstrate that the increases in SMN protein levels induced by SMN-C1 treatment in the spinal cord of SMNΔ7 SMA mice are associated with enhanced SMN function as indicated by the correction of snRNP biogenesis and downstream RNA processing defects caused by SMN deficiency. Furthermore, we demonstrate that increased SMN protein levels and SMN protein function are associated with reduced neuromuscular pathology, improved motor function, body weight gain and increased survival. Administration of SMN-C1 at a dose of 0.1 mg/kg IP from PND3 through PND23 followed by a dose of 0.6 mg/kg PO from PND24 onward resulted in robust improvement of survival and body weight gain deficits of SMA mice (Fig. 4A and B), although disease phenotypes were only partially corrected, as revealed by moderate improvement of tail necrosis and less effective prevention of hallmarks of SMA neuromuscular pathology such as motor neuron loss and NMJ denervation. SMN-C1 administered at a dose of 0.1 mg/kg IP from PND3 through PND9 increased SMN protein levels by 66% in the brain and by 35% in the spinal cord relative to vehicle-treated controls indicating that this extent of SMN protein increase is beneficial, but not optimal. Administration of SMN-C1 at a dose of 0.3 mg/kg IP from PND3 through PND23 followed by a dose of 2 mg/kg PO from PND24 onward resulted in robustly improved survival and body weight gain as well as significantly reduced peripheral necrosis (tail, pinna, tissue surrounding the eye). At a dose of 0.3 mg/kg IP dosed from PND3 through PND9, the levels of SMN protein in the brain and spinal cord were increased by ∼100% relative to those in vehicle-dosed mice. Given that a 100% increase relative to vehicle is still well below the levels of CNS SMN protein in HET mice, which are 500% above those in the vehicle-dosed mice, SMN protein levels do not need to be completely restored to provide a beneficial effect.

In summary, we have shown that administration of SMN-C1 to SMNΔ7 SMA mice results in long-term survival. Although prolonged survival was seen at the lower doses, the phenotype was only partially corrected as evidenced by necrosis of tail, pinna and tissues surrounding the eye, reduced protection from motor neuron loss and NMJ denervation, and reduced protection from muscle atrophy. In contrast, the SMA phenotype was robustly improved at the higher dose. Specifically, at a dose of SMN-C1 that increased SMN protein levels by 100% resulted not only in long-term survival and increased body weight gain, but also in the restoration of the SMN-dependent RNA processing, improved histopathology of the spinal cord and NMJ, and improved NMJ function. These results contribute to the design and planning of clinical development of compounds that correct *SMN2* exon 7 splicing.

Materials and Methods

All animal studies were performed under IACUC approved protocols at AAALAC-certified animal facilities.

Pharmacokinetic studies in animals

The pharmacokinetics of SMN-C1 was evaluated in wild-type FVB/N mice (The Jackson Laboratory, Bar Harbor Maine). For

oral dosing of adult mice, SMN-C1 was formulated as a suspension in 0.5% hydroxypropylmethyl cellulose (HPMC) with 0.1% Tween 80 and administered by gavage at a dose of 10 mg/kg at 5 ml/kg. For intraperitoneal dosing of 10-day-old mice, SMN-C1 was formulated in dimethyl sulfoxide (DMSO) and administered at a dose of 10 mg/kg at 2.5 ml/kg. Blood was collected by terminal cardiac puncture at specified time points (three mice per time point), and centrifuged to collect plasma. Brain tissue was collected at the time of blood collection and homogenized in water. The concentrations of test compound in plasma and brain tissue were quantified by liquid chromatography-tandem mass spectrometry (LC-MS/MS). Briefly, the plasma and tissue homogenate samples were treated with acetonitrile-methanol mixture containing an internal standard that is a close structural analog of the test compounds. The treated plasma and brain homogenate samples were centrifuged and the supernatant was collected and analyzed using electro-spray LC-MS/MS.

SMA mice

Animals were kept in a controlled vivarium at ~25°C and ~50% humidity with a 12 h light/dark photoperiod and monitored for health. Mice had free access to food and water. The original breeding pairs of SMNΔ7 SMA mice were purchased from The Jackson Laboratory [(*FVB.Cg-Tg(SMN2*delta7)4299Ahmb Tg(SMN2)89Ahmb Smn1tm1Msd/J*; stock number 005025)] (25). The original breeding pairs of the C/C- allele mice [*FVB.129(B6)-Smn1*$^{tm5(Smn1/SMN2)Mrph}$*/J*; stock number 008604] (24) were obtained from The Jackson Laboratory. Both colonies were maintained by interbreeding carrier mice, and the offspring were genotyped as described below.

Genotyping

SMNΔ7 SMA mice were identified by genotyping at PND2 using a PCR-based assay using genomic DNA from tail biopsies. Crude genomic DNA was released from a 0.5 cm tail clips by denaturing in 25 mM NaOH and 0.2 mM ethylenediaminetetraacetic acid buffer for 1 h at 98°C and then neutralizing with the addition of an equal volume of 40 mM Tris–HCl (pH 5.5). PCR was performed using Platinum TaqHiFi PCR supermix (Thermo Fisher Scientific cat. number 12532-016), two forward primers, and one common reverse primer to obtain a 250 bp product for the wild-type allele and a 180 bp product for the mutant allele. Primer sequences were GGTTGATCTAGGGACTTTGAGC (Primer 1); CTCTCTTTCTTTACA AAATGTATGACC (Primer 2) and CATGCTGGGTACATGAAAACC (Primer 3). PCR was performed for 1 cycle of 94°C for 2 min followed by 32 cycles of 94°C for 30 sec, 57°C for 30 s and 68°C for 60 s.

RNA analysis

The total RNA was isolated using Trizol (Thermo Fisher Scientific, cat. no. 15596-026) followed by digestion with RNase-free DNase I (Thermo Fisher Scientific, cat. no. AM2222). For mRNA analysis, mixture of oligo-dT primers and random hexamers was used to generate cDNA using Advantage RT-for-PCR kit (Clontech) and 1 μg of total RNA following the manufacturer's instructions. For spliceosomal snRNA analysis, snRNA-specific reverse primers were used in the RT reaction according to a previous study (51). All primers and probes used in RT-qPCR and northern blot experiments were previously described (28–30,53,54).

Quantification of SMN protein in animal tissues

To measure increases in SMN protein *in vivo* in a mouse model of Type III SMA, adult C/C-allele mice were treated daily for 10 days. One hour after the 10th dose, mice were euthanized and tissues were collected. To measure increases in SMN protein *in vivo* in a mouse model of Type I SMA, 3-day old (PND3) SMNΔ7 SMA mice were dosed daily from PND3 through PND9 or PND3 through PND11, as specified for the study. One hour after the last dose, mice were euthanized and tissues were collected. To measure increases in SMN protein *in vivo*, tissue samples were collected and homogenized on the TissueLyzer II (Qiagen) in buffer comprising 20 mM Tris-HCl pH 7.5, 150 mM NaCl, 1 mM EDTA, 1% NP-40, 1% sodium deoxycholate, with complete protease inhibitor cocktail (Roche). The samples were then centrifuged for 20 min at 14 000×*g* in a microcentrifuge. The homogenates were transferred to a 96-well plate and were diluted in RIPA buffer. Samples were run in duplicate and averaged. SMN protein was quantified using homogeneous time-resolved fluorescence (HTRF, Cisbio Bioassays) as previously published (20). For the HTRF assay, 35 μl of tissue homogenate were transferred to a 384-well plate containing 5 μl of the antibody solution [1:100 dilution of anti-SMN d2 and anti-SMN cryptate (Cisbio)]. The plate was incubated overnight at room temperature. Fluorescence was measured at 665 and 620 nm on an EnVision multilabel plate reader (Perkin Elmer). Total protein content was quantified in each tissue homogenate using the bicinchoninic acid protein assay according to the manufacturer's protocol.

The HTRF signal for SMN protein was normalized to the total protein concentration for each sample generating the delta F SMN signal/total protein. The percent increase was calculated as:

$$100 \times (\text{treated} - \text{vehicle})/\text{vehicle}$$

where the vehicle is the mean SMN/total protein for the vehicle-dosed group and treated is the SMN/total protein for each compound-dosed animal. Statistical differences between groups were determined using ANOVA (multiple comparisons versus vehicle; GraphPad, Carey, NC, USA).

SMNΔ7 SMA mouse survival studies

Homozygous SMNΔ7 SMA mice were dosed IP with SMN-C1 or vehicle (100% DMSO) once per day from PND3 until the dosing regimen was switched on PND24 to an oral dose 3-fold higher twice per day in 0.5% HPMC and 0.1% Tween 80. Litters were randomized across groups, with 9–15 mice per group. Body weight and survival were assessed daily. The group size was powered to show statistically significant differences in survival, body weight, righting-reflex and tail length (optimal group size estimated using SigmaStat 3.0, power = 80%). Survival analysis was done using GraphPad Prism (log-rank test) and a *P*-value of <0.05 was considered as significant.

Survival study 1: SMN-C1 was administered by IP dosing (at 0.1 or 0.3 mg/kg IP, qd) from PND3 through PND23. From PND24 through PND59, mice were treated by oral gavage (0.3 or 1 mg/kg bid, PO, Monday to Friday and 0.6 or 2 mg/kg qd PO on Saturday and Sunday). After PND60, mice were dosed at 0.6 or 2 mg/kg qd PO, respectively.

Survival study 2: SMN-C1 was administered by IP dosing (at 1, 3 or 10 mg/kg) initiated at PND3 and continued through PND29. From PND30 onward, mice were treated by oral gavage (3,10 or 30 mg/kg bid, PO).

Assessment of motor neuron pathology

The *longissimus capitis*, *splenius capitis* and *serratus posterior inferior* muscles were dissected and teased into layers 5–10 fibers thick.

Pre-synaptic nerve terminals were labeled with anti-NF (Millipore) and anti-synaptophysin (Thermo Fisher) antibodies, and post-synaptic acetylcholine receptors were labeled with α-bungarotoxin (Thermo Fisher). NMJs were visualized and quantified by epifluorescence or confocal microscopy. NMJs were considered fully innervated if the pre-synaptic nerve terminal completely co-localized with the post-synaptic endplate, and the innervation percentage was calculated as the number of fully innervated NMJs divided by the total number of NMJs quantified. Neurofilament accumulation was defined as NF staining that occupied >25% of the motor endplate area (35).

To examine central synapses, lumbar cord spinal segments 3–5 (L3–5) were dissected and sectioned at 80 µm. Spinal cord sections were stained with anti-ChAT (Millipore) and anti-vGlut1 (Synaptic Systems) antibodies, and imaged at 1 µm intervals using × 100 oil-immersion objectives on the Zeiss LSM confocal microscope. The number of primary proprioceptive afferents was quantified as vGlut1-positive puncta abutting on the soma and proximal dendrites of motor neurons.

Electrophysiological recordings from NMJs

Conventional intracellular recordings were performed as described previously (35). The EDL and *splenius capitis* muscles with their nerves attached were dissected in normal Ringer's solution and were pre-incubated in 2–3 µM µ-conotoxin for 30 min to block muscle contraction. The recording was then performed in toxin-free Ringer's solution. EPPs were elicited by 1 Hz train through a suction electrode and recorded via a glass pipette filled with 3 M KCl. The EPP amplitudes were normalized to −50 mV and corrected for non-linear summation. Data were acquired and analyzed using the pClamp8 software and Mini Analysis software. The mean quantal content was calculated by the direct method (41). A one-way ANOVA was used for comparison of means across groups (multiple comparisons versus vehicle).

Motor function evaluation of neonatal SMNΔ7 SMA mice

The righting reflex evaluates the time (in seconds) that it takes an animal to right itself when placed on its back. The animal was given a maximum of 30 s to complete the test. Three trials were recorded for each mouse, and the mean of three trials/animal was then averaged across the group.

The geotaxis assay measures motor coordination and the vestibular system and tests the ability of the animal to orient itself when placed face down on an inclined platform (~35° inclination). Animals were given a maximum of 60 s to complete the test.

The tube test is designed to test hind-limb strength and general body muscle tone in neonatal mice (age PND2–PND23) (55). The test is performed in two consecutive trials. There is no time limit for either trial. In each trial, the mouse is placed face down, hanging by its hind-limbs in a plastic 50 ml centrifuge tube (hence the name tube test). Three parameters are evaluated: (i) time spent hanging (s); (ii) number of pulls (to escape the tube) and (iii) hind-limb score (HLS) (ranging from 0 to 4; 0 indicates paralysis and 4 indicates normal tone). These parameters are then included in an equation that provides a score referred to as the tube test score (TTS) (TTS = [(time hanging) + (# pulls × 10)] × (HLS + 1)/4.

Supplementary Material

Supplementary Material is available at *HMG* online.

Acknowledgements

The authors thank William Lennox, OnkarVaze and Mandar Dali for support with formulation; Guangming Chen and Anthony Turpoff for providing SMN-C1, and Joseph Colacino for reviewing the manuscript, and Julia Paget for help with figures.

Conflict of Interest statement. X.Z., A.M., J.S., S.Y., J.P., J.N., G.K., E.W., A.D., N.N. and M.W. are financially compensated as employees of PTC Therapeutics. H.R. and F.M. are financially compensated as employees of F. Hoffmann-La Roche, Ltd.

Funding

Work in the C.-P.K. and M.W. Laboratories was supported by the Spinal Muscular Atrophy Foundation, and work in the L.P. laboratory was supported by a grant from NIH-National Institute of Neurological Disorders and Stroke (R01NS069601). Funding to pay the Open Access publication charges for this article was provided by PTC Therapeutics, Inc.

References

1. Burghes, A.H. and Beattie, C.E. (2009) Spinal muscular atrophy: why do low levels of survival motor neuron protein make motor neurons sick? *Nat. Rev. Neurosci.*, **10**, 597–609.
2. Tisdale, S. and Pellizzoni, L. (2015) Disease mechanisms and therapeutic approaches in spinal muscular atrophy. *J. Neurosci.*, **35**, 8691–8700.
3. Lefebvre, S., Burglen, L., Reboullet, S., Clermont, O., Burlet, P., Viollet, L., Benichou, B., Cruaud, C., Millasseau, P., Zeviani, M. *et al.* (1995) Identification and characterization of a spinal muscular atrophy-determining gene. *Cell*, **80**, 155–165.
4. Ogino, S., Gao, S., Leonard, D.G., Paessler, M. and Wilson, R.B. (2003) Inverse correlation between SMN1 and SMN2 copy numbers: evidence for gene conversion from SMN2 to SMN1. *Eur. J. Hum. Genet.*, **11**, 275–277, (see Addendum in vol. 11; 723).
5. Lorson, C.L., Hahnen, E., Androphy, E.J. and Wirth, B. (1999) A single nucleotide in the SMN gene regulates splicing and is responsible for spinal muscular atrophy. *Proc. Natl Acad. Sci. USA*, **96**, 6307–6311.
6. Monani, U.R., Lorson, C.L., Parsons, D.W., Prior, T.W., Androphy, E.J., Burghes, A.H. and McPherson, J.D. (1999) A single nucleotide difference that alters splicing patterns distinguishes the SMA gene SMN1 from the copy gene SMN2. *Hum. Mol. Genet.*, **8**, 1177–1183.
7. Cho, S. and Dreyfuss, G. (2010) Adegron created by SMN2 exon 7 skipping is a principal contributor to spinal muscular atrophy severity. *Genes Dev.*, **24**, 438–442.
8. Burnett, B.G., Muñoz, E., Tandon, A., Kwon, D.Y., Sumner, C.J. and Fischbeck, K.H. (2009) Regulation of SMN protein stability. *Mol. Cell Biol.*, **29**, 1107–1115.
9. Feldkötter, M., Schwarzer, V., Wirth, R., Wienker, T.F. and Wirth, B. (2002) Quantitative analyses of SMN1 and SMN2 based on real-time lightCycler PCR: fast and highly reliable carrier testing and prediction of severity of spinal muscular atrophy. *Am. J. Hum. Genet.*, **70**, 358–368.
10. Wirth, B., Brichta, L., Schrank, B., Lochmüller, H., Blick, S., Baasner, A. and Heller, R. (2006) Mildly affected patients with spinal muscular atrophy are partially protected by an increased SMN2 copy number. *Hum. Genet.*,**119**, 422–428.
11. Crawford, T.O. and Pardo, C.A. (1996) The neurobiology of childhood spinal muscular atrophy. *Neurobiol. Dis.*, **3**, 97–110.

12. Pellizzoni, L. (2007) Chaperoning ribonucleoprotein biogenesis in health and disease. *EMBO Rep.*, **8**, 340–345.
13. Li, D.K., Tisdale, S., Lotti, F. and Pellizzoni, L. (2014) SMN control of RNP assembly: from post-transcriptional gene regulation to motor neuron disease. *Semin. Cell Dev. Biol.*, **32**, 22–29.
14. Zhou, J., Zheng, X. and Shen, H. (2012) Targeting RNA-splicing for SMA treatment. *Mol. Cells*, **33**, 223–228.
15. Bebee, T.W., Dominguez, C.E. and Chandler, D.S. (2012) Mouse models of SMA: tools for disease characterization and therapeutic development. *Hum. Genet.*,**131**, 1277–1293.
16. Hua, Y., Sahashi, K., Rigo, F., Hung, G., Horev, G., Bennett, C.F. and Krainer, A.R. (2011) Peripheral SMN restoration is essential for long-term rescue of a severe spinal muscular atrophy mouse model. *Nature*, **478**, 123–126.
17. Hua, Y., Liu, Y.H., Sahashi, K., Rigo, F., Bennett, C.F. and Krainer, A.R. (2015) Motor neuron cell-nonautonomous rescue of spinal muscular atrophy phenotypes in mild and severe transgenic mouse models. *Genes. Dev.*, **29**, 288–297.
18. Osman, E.Y., Miller, M.R., Robbins, K.L., Lombardi, A.M., Atkinson, A.K., Brehm, A.J. and Lorson, C.L. (2014) Morpholino antisense oligonucleotides targeting intronic repressor Element1 improve phenotype in SMA mouse models. *Hum. Mol. Genet.*, **23**, 4832–4845.
19. Porensky, P.N., Mitrpant, C., McGovern, V.L., Bevan, A.K., Foust, K.D., Kaspar, B.K., Wilton, S.D. and Burghes, A.H. (2012) A single administration of morpholino antisense oligomer rescues spinal muscular atrophy in mouse. *Hum. Mol. Genet.*, **21**, 1625–1638.
20. Naryshkin, N.A., Weetall, M., Dakka, A., Narasimhan, J., Zhao, X., Feng, Z., Ling, K.K., Karp, G.M., Qi, H., Woll, M.G. *et al.* (2014) Motor neuron disease. SMN2 splicing modifiers improve motor function and longevity in mice with spinal muscular atrophy. *Science*, **345**, 688–693.
21. Angelozzi, C., Borgo, F., Tiziano, F.D., Martella, A., Neri, G. and Brahe, C. (2008) Salbutamol increases SMN mRNA and protein levels in spinal muscular atrophy cells. *J. Med. Genet.*, **45**, 29–31.
22. Palacino, J., Swalley, S.E., Song, C., Cheung, A.K., Shu, L., Zhang, X., Van Hoosear, M., Shin, Y., Chin, D.N., Keller, C.G. *et al.* (2015) SMN2 splice modulators enhance U1-pre-mRNA association and rescue SMA mice. *Nat. Chem. Biol.*, **11**, 511–517.
23. Feng, Z., Ling, K.K., Zhao, X., Zhou, C., Karp, G., Welch, E.M., Naryshkin, N., Ratni, H., Chen, K.S., Metzger, F. *et al.* (2016) Pharmacologically induced mouse model of adult spinal muscular atrophy to evaluate effectiveness of therapeutics after disease onset. *Hum. Mol. Genet.*, **25**, 964–975.
24. Osborne, M., Gomez, D., Feng, Z., McEwen, C., Beltran, J., Cirillo, K., El-Khodor, B., Lin, M.Y., Li, Y., Knowlton, W.M. *et al.* (2012) Characterization of behavioral and neuromuscular junction phenotypes in a novel allelic series of SMA mouse models. *Hum. Mol. Genet.*, **21**,4431–4447.
25. Le, T.T., Pham, L.T., Butchbach, M.E., Zhang, H.L., Monani, U.R., Coovert, D.D., Gavrilina, T.O., Xing, L., Bassell, G.J. and Burghes, A.H. (2005) SMNDelta7, the major product of the centromeric survival motor neuron (SMN2) gene, extends survival in mice with spinal muscular atrophy and associates with full-length SMN. *Hum. Mol. Genet.*, **14**, 845–857.
26. Gabanella, F., Butchbach, M.E., Saieva, L., Carissimi, C., Burghes, A.H. and Pellizzoni, L. (2007) Ribonucleoprotein assembly defects correlate with spinal muscular atrophy severity and preferentially affect a subset of spliceosomalsnRNPs. *PLoS One*, **2**, e921.
27. Zhang, Z., Lotti, F., Dittmar, K., Younis, I., Wan, L., Kasim, M. and Dreyfuss, G. (2008) SMN deficiency causes tissue-specific perturbations in the repertoire of snRNAs and widespread defects in splicing. *Cell*, **133**, 585–600.
28. Tisdale, S., Lotti, F., Saieva, L., Van Meerbeke, J.P., Crawford, T.O., Sumner, C.J., Mentis, G.Z. and Pellizzoni, L. (2013) SMN is essential for the biogenesis of U7 small nuclear ribonucleoprotein and 3'-end formation of histone mRNAs. *Cell Rep.*, **5**, 1187–1195.
29. Lotti, F., Imlach, W.L., Saieva, L., Beck, E.S., Hao, L.T., Li, D.K., Jiao, W., Mentis, G.Z., Beattie, C.E., McCabe, B.D. and Pellizzoni, L. (2012) An SMN-dependent U12 splicing event essential for motor circuit function. *Cell*, **151**, 440–454.
30. Ruggiu, M., McGovern, V.L., Lotti, F., Saieva, L., Li, D.K., Kariya, S., Monani, U.R., Burghes, A.H. and Pellizzoni, L. (2012) A role for SMN exon 7 splicing in the selective vulnerability of motor neurons in spinal muscular atrophy. *Mol. Cell Biol.*, **32**, 126–138.
31. Fallini, C., Bassell, G.J. and Rossoll, W. (2012) Spinal muscular atrophy: the role of SMN in axonal mRNA regulation. *Brain Res.*, **1462**, 81–92.
32. Sleigh, J.N., Barreiro-Iglesias, A., Oliver, P.L., Biba, A., Becker, T., Davies, K.E., Becker, C.G. and Talbot, K. (2014) Chondrolectin affects cell survival and neuronal outgrowth in in vitro and in vivo models of spinal muscular atrophy. *Hum. Mol. Genet.*, **23**, 855–869.
33. Hsieh-Li, H.M., Chang, J.G., Jong, Y.J., Wu, M.H., Wang, N.M., Tsai, C.H. and Li, H. (2000) A mouse model for spinal muscular atrophy. *Nat. Genet.*, **24**, 66–70.
34. Hua, Y., Sahashi, K., Hung, G., Rigo, F., Passini, M.A., Bennett, C.F. and Krainer, A.R. (2010) Antisense correction of SMN2 splicing in the CNS rescues necrosis in a type III SMA mouse model. *Genes Dev.*, **24**, 1634–1644.
35. Passini, M.A., Bu, J., Roskelley, E.M., Richards, A.M., Sardi, S.P., O'Riordan, C.R., Klinger, K.W., Shihabuddin, L.S. and Cheng, S.H. (2010) CNS-targeted gene therapy improves survival and motor function in a mouse model of spinal muscular atrophy. *J. Clin. Invest.*, **120**, 1253–1264.
36. Ling, K.K., Lin, M.Y., Zingg, B., Feng, Z. and Ko, C.P. (2010) Synaptic defects in the spinal and neuromuscular circuitry in a mouse model of spinal muscular atrophy. *PLoS One*, **5**, e15457.
37. Mentis, G.Z., Blivis, D., Liu, W., Drobac, E., Crowder, M.E., Kong, L., Alvarez, F.J., Sumner, C.J. and O'Donovan, M.J. (2011) Early functional impairment of sensory-motor connectivity in a mouse model of spinal muscular atrophy. *Neuron*, **69**, 453–467.
38. Ling, K.K., Gibbs, R.M., Feng, Z. and Ko, C.P. (2012) Severe neuromuscular denervation of clinically relevant muscles in a mouse model of spinal muscular atrophy. *Hum. Mol. Genet.*, **21**, 185–195.
39. Cifuentes-Diaz, C., Nicole, S., Velasco, M.E., Borra-Cebrian, C., Panozzo, C., Frugier, T., Millet, G., Roblot, N., Joshi, V. and Melki, J. (2002) Neurofilament accumulation at the motor endplate and lack of axonal sprouting in a spinal muscular atrophy mouse model. *Hum. Mol. Genet.*, **11**, 1439–1447.
40. Kariya, S., Park, G.H., Maeno-Hikichi, Y., Leykekhman, O., Lutz, C., Arkovitz, M.S., Landmesser, L.T. and Monani, U.R. (2008) Reduced SMN protein impairs maturation of the neuromuscular junctions in mouse models of spinal muscular atrophy. *Hum. Mol. Genet.*, **17**, 2552–2569.
41. Murray, L.M., Comley, L.H., Thomson, D., Parkinson, N., Talbot, K. and Gillingwater, T.H. (2008) Selective vulnerability of motor neurons and dissociation of pre- and post-synaptic pathology at the neuromuscular junction in mouse models of spinal muscular atrophy. *Hum. Mol. Genet.*, **17**, 949–962.
42. Cruz, L.J., Gray, W.R., Olivera, B.M., Zeikus, R.D., Kerr, L., Yoshikami, D. and Moczydlowski, E. (1985) Conusgeographus

toxins that discriminate between neuronal and muscle sodium channels. *J. Biol. Chem.*, **260**, 9280–9288.
43. DelCastillo, J. and Katz, B. (1954) Quantal components of the end-plate potential. *J. Physiol.*, **124**, 560–573.
44. Saunders, N.R., Liddelow, S.A. and Dziegielewska, K.M. (2012) Barrier mechanisms in the developing brain. *Front. Pharmacol.*, **3**, 46.
45. Hart, S.N., Cui, Y., Klaassen, C.D. and Zhong, X. (2009) Three patterns of cytochrome P450 gene expression during liver maturation in mice. *Drug Metab. Dispos.*, **37**, 116–121.
46. Peng, L., Cui, J.Y., Yoo, B., Gunewardena, S.S., Lu, H., Klaassen, C.D. and Zhong, X.B. (2013) RNA-sequencing quantification of hepatic ontogeny of phase-I enzymes in mice. *Drug Metab. Dispos.*, **41**, 2175–2186.
47. Bevan, A.K., Duque, S., Foust, K.D., Morales, P.R., Braun, L., Schmelzer, L., Chan, C.M., McCrate, M., Chicoine, L.G., Coley, B.D. *et al.*(2011) Systemic gene delivery in large species for targeting spinal cord, brain, and peripheral tissues for pediatric disorders. *Mol. Ther.*, **19**, 1971–1980.
48. Heier, C.R., Satta, R., Lutz, C. and DiDonato, C.J. (2010) Arrhythmia and cardiac defects are a feature of spinal muscular atrophy model mice. *Hum. Mol. Genet.*, **19**, 3906–3918.
49. Hamilton, G. and Gillingwater, T.H. (2013) Spinal muscular atrophy: going beyond the motor neuron. *Trends Mol. Med.*, **19**, 40–50.
50. Shababi, M., Lorson, C.L. and Rudnik-Schöneborn, S.S. (2014) Spinal muscular atrophy: a motor neuron disorder or a multi-organ disease? *J. Anat.*, **224**, 15–28.
51. Bowerman, M., Swoboda, K.J., Michalski, J.P., Wang, G.S., Reeks, C., Beauvais, A., Murphy, K., Woulfe, J., Screaton, R.A., Scott, F.W. and Kothary, R. (2012) Glucose metabolism and pancreatic defects in spinal muscular atrophy. *Ann. Neurol.*, **72**, 256–268.
52. Araujo, A.P., Araujo, M. and Swoboda, K.J. (2009) Vascular perfusion abnormalities in infants with spinal muscular atrophy. *J. Pediatr.*, **155**, 292–294.
53. Workman, E., Saieva, L., Carrel, T.L., Crawford, T.O., Liu, D., Lutz, C., Beattie, C.E., Pellizzoni, L. and Burghes, A.H. (2009) A SMN missense mutation complements SMN2 restoring snRNPs and rescuing SMA mice. *Hum. Mol. Genet.*, **18**, 2215–2229.
54. Li, D.K., Tisdale, S., Espinoza-Derout, J., Saieva, L., Lotti, F. and Pellizzoni, L. (2013) A cell system for phenotypic screening of modifiers of SMN2 gene expression and function. *PLoS One*, **8**, e71965.
55. El-Khodor, B.F., Edgar, N., Chen, A., Winberg, M.L., Joyce, C., Brunner, D., Suárez-Fariñas, M. and Heyes, M.P. (2008) Identification of a battery of tests for drug candidate evaluation in the SMNDelta7 neonate model of spinal muscular atrophy. *Exp. Neurol.*, **212**, 29–43.